Mathematical Formulation and Analysis of Static and Dynamic Performance Characteristics of Lobed Fluid Film Bearing Operating with Nanolubricant using Variable Viscosity Approach

Ashutosh Kumar[1*],Alka Kumari[2],Dr.A.M.Arun Mohan[3],Ashish Gaurav [4] & Dr. Krupal Prabhakar Pawar [5]

[1]New Government Polytechnic,Patna, Bihar, India.

[2]New Government Polytechnic, Patna, Bihar, India.

[3]Associate Professor,Department of Civil Engineering,Sethu Institute of Technology,Pulloor,Kariapatti,Tamilnadu,India.

[4]Department of Mechanical Engineering, National Institute of Technology, Patna, Bihar, India.

[5] Assistant Professor, Department of Mechanical Engineering, Rajiv Gandhi College of Engineering, Karjule Harya Tal.Parner, Dist. Ahilyanagar, Maharashtra, India.

Abstract

The static and dynamic performance parameters of a three-lobe fluid film bearing operating with a TiO_2-based non-Newtonian lubricant are analyzed. The Krieger-Dougherty model is employed to calculate the viscosity of the nanolubricant at a fixed nanoparticle concentration dispersed in the base lubricant. The Reynolds equation is modified to incorporate the couple-stress effect, and the Finite Difference Method (FDM) is used to solve it to determine various performance parameters. For varying nanoparticle concentrations in the base lubricant, the direct and cross-coupled dynamic coefficients (stiffness and damping) are evaluated. The results indicate that the flow coefficient and load-carrying capacity increase, while the friction variable decreases, without compromising the stability of the three-lobe fluid film bearing operating with the TiO_2-based non-Newtonian lubricant. Furthermore, the dynamic coefficients and attitude angle remain unaffected by the nanoparticle concentration for a fixed couple-stress parameter.

Keywords: Journal Bearing, Hydrodynamic Lubrication, Nanolubricant, Lobe, Load Carrying Capacity, Friction Variable, Finite Difference Method, Sommerfeld Number.

NOMENCLATURE

C = Radial clearance in meter

C_m = Film thickness for a cantered shaft in meter

$C_{xx}, C_{xz}, C_{zx}, C_{zz}$ = Damping coefficients in Ns/m

$\bar{C}_{xx}, \bar{C}_{xz}, \bar{C}_{zx}, \bar{C}_{zz}$ = Damping coefficients in non-dimensional form $\bar{C}_{xx} = C_{xx}\left(\omega C/W\right)$

e = Eccentricity in meter

ε = Eccentricity ratio $\varepsilon = e/C$

e_1, e_2, e_3 = Eccentricity for each lobe in meter

h = Oil-film thickness in meter

$\bar{h}$ = Film thicknessnon-dimensional form $\bar{h} = h/C$

$K_{xx}, K_{xz}, K_{zx}, K_{zz}$ = Stiffness coefficients in N/m

$\bar{K}_{xx}, \bar{K}_{xz}, \bar{K}_{zx}, \bar{K}_{zz}$ = Stiffness coefficients in non-dimensional form $\bar{K}_{xx} = K_{xx}\left(C/W\right)$

L = Bearing length in m

D_d = Depth of pressure dam in meter

$\bar{D}_d$ = Depth of non-dimensional pressure dam $\bar{D}_d = D/C$

D_w = Width of pressure dam meter

$\bar{D}_w$ = Width of non-dimensional pressure dam $\bar{D}_w = D_w/L$

R_d = Depth of relief track meter

$\bar{R}_d$ = Depth of non-dimensional relief track $\bar{R}_d = R_d/C$

R_w = Width of Relief track in meter

$\bar{R}_w$ = Depth of non-dimensional relief track $\bar{R}_w = R_w/L$

m = Rotor mass per bearing in kg

ω = journal Angular velocity in rad/s

$\bar{M}$ = Mass parameter $\bar{M} = mC\omega^2/W$

N = Journal speed in rps

D = Journal diameter in meter

p = Pressure $\left(p = W/LD\right)$ in N/m^2

$\bar{p}$ = film pressure non-dimensional form $\bar{p} = pC^2/6\mu UR$

R = Radius of bearing in meter

U = Sliding speed in m/s

$\bar{\mu}$ = Effective viscosity

ψ = Attitude angle in radian

ϕ = Volume fraction of solid additive

S = Sommerfeld Number $S = \mu N / p \left(R/C\right)^2$

$\bar{f}$ = Friction variable in non-dimensional form $\bar{f} = f\left(R/C\right)$

μ_{nf} = Nano lubricant viscosity

μ_{bf} =Base lubricant viscosity

W = Load capacity in N

$\bar{W}$ = Load capacity in non-dimensional form $\bar{W} = WC^2 / 6\mu UR^2 L$

$\bar{p}_1, \bar{p}_2$ = Perturbed pressure

δ = Ellipticity ratio $\delta = d/C$

d = Distance between lobe centre and centre of entire bearing geometry in meter

t = time, s

τ = time in non-dimensional form $\tau = \omega_p t$

ω_p = Whirling velocity in rad/s

$\bar{\omega}_j$ = Speed parameter

W_x = Resultant load in vertical direction in N

W_z = Resultant load in horizontal direction in N

θ_s = Groove starting angle

θ_e = Groove end angle

θ_r = Film cavitation angle

$\bar{Q}$ = Flow coefficient

1. INTRODUCTION

Modern tribologists face significant challenges due to the increasing speed and load demands in practical applications, necessitating the development of advanced solutions. Multilobe bearings were introduced to address the limitations of plain journal bearings, such as high friction, low load-carrying capacity, stability issues, and low stiffness. Researchers (e.g., Soni et al. [1], Lund and Thomson [2], Singh and Gupta [3], Kumar et al. [4]) have demonstrated that multilobe bearings offer superior stability, making them ideal for high-speed machinery.

In addition to geometric improvements, the properties of lubricating oils have been extensively studied. It has been shown that dispersing nano-solid particles in base lubricants significantly enhances lubrication performance. The micro-continuum theory of couple stress fluids has also been explored (Sylvester and Ariman [5, 6], Stokes [7]), focusing on fluids containing fine solid particles (Lin [8], Wang et al. [9, 10], Mokhiyamer et al. [11] and Lin [12]). These studies indicate substantial improvements in stability and load-carrying capacity for finite fluid film bearings.

This study investigates the effects of viscosity variations in lubricants caused by different volume fractions of TiO_2 nanoparticles and their impact on the static and dynamic performance of three-lobe journal bearings. The Krieger-Dougherty model is used to account for viscosity variation, while the couple stress parameter is kept constant. The modified Reynolds equation, incorporating the couple stress parameter, is solved using the Gauss-Seidel method with successive over-relaxation on a finite grid, comparing pressure profiles for various nanoparticle concentrations.

2. THEORY

The centers of lobes 1 and 2 of a three-lobe journal bearing are shown in Figure 1. A 10^0 oil supply hole ensures continuous lubrication, positioned 180° apart. The study considers an ellipticity ratio (δ) of 0.5, defined as $\delta = \frac{e_p}{C}$, where (e_p) represents the distance between the bearing center and lobe center. While individual lobes are circular, the bearing overall is non-circular.

The study employs the Krieger-Dougherty Viscosity Model, which relates the effective viscosity of nanofluids to the solid nanoparticle concentration in the base lubricant. This model is given by [13]:

$$\bar{\mu} = \frac{\mu_{nf}}{\mu_{bf}} = \left(1 - \frac{\phi}{\phi_m}\right)^{-[\eta]\phi m} \tag{1}$$

The material constant responsible for the couple stress properties of a non-Newtonian lubricant is denoted as η. The characteristic length (l) of solid additives in a nanolubricant is defined as $l = \sqrt{\frac{\eta}{\mu}}$. The influence of the couple stress parameter on the performance characteristics of the bearing system is evaluated using a non-dimensional parameter $d = \frac{l}{C}$.

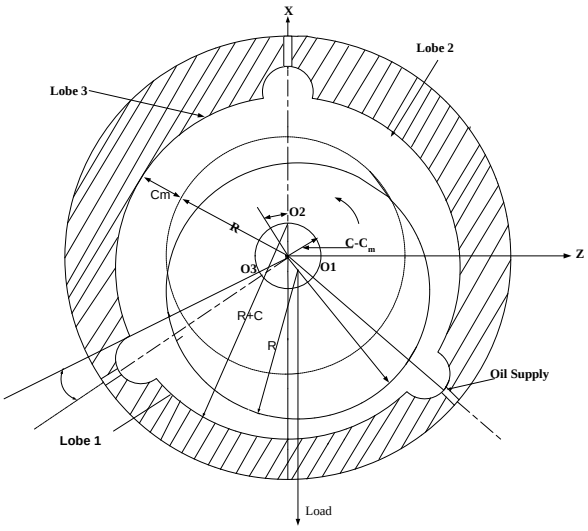

Figure 1: Three-lobejournal bearing.

In current study, the concentration of nanoparticles is varied (ϕ=0.001, 0.005, 0.01 and 0.02)while the couple stress parameter remains fixed at d =0.4. The performance characteristics of a three-lobe fluid film bearing are significantly influenced by the higher concentrations of solid nanoparticles in the base fluid. The eccentricity ratios for each individual lobe are expressed as:

$$\varepsilon_1 = \sqrt{\varepsilon^2 + \delta^2 + 2\varepsilon\delta\cos(\phi)} \tag{2}$$

$$\varepsilon_2 = \sqrt{\varepsilon^2 + \delta^2 - 2\varepsilon\delta\cos\left(\frac{\pi}{3} + \phi\right)} \tag{3}$$

$$\varepsilon_3 = \sqrt{\varepsilon^2 + \delta^2 - 2\varepsilon\delta\cos\left(\frac{\pi}{3} - \phi\right)} \tag{4}$$

Similarly, the attitude angle for individual lobe might be expressed as:

$$\phi_1 = \tan^{-1}\left(\frac{\varepsilon\sin\phi}{\delta + \varepsilon\cos\phi}\right) \tag{5}$$

$$\phi_2 = \frac{2\pi}{3} - \tan^{-1}\left(\frac{\varepsilon\sin\left(\frac{\pi}{3} + \phi\right)}{\delta - \varepsilon\cos\left(\frac{\pi}{3} + \phi\right)}\right) \tag{6}$$

$$\phi_3 = -\left(\frac{2\pi}{3} - \tan^{-1}\left(\frac{\varepsilon \sin\left(\frac{\pi}{3} - \phi\right)}{\delta - \varepsilon \cos\left(\frac{\pi}{3} - \phi\right)} \right) \right) \tag{7}$$

For couple stress model the Reynolds equation can be modified as [14]:

$$\frac{\partial}{\partial x}\left[f\left(h,d\right)\frac{\partial p}{\partial x}\right] + \frac{\partial}{\partial z}\left[f\left(h,d\right)\frac{\partial p}{\partial z}\right] = 6\mu U\frac{\partial h}{\partial x} + 12\mu\frac{\partial h}{\partial t} \tag{8}$$

where,

$$f\left(h,d\right) = h^3 - 12d^2h + 24d^3\tanh\left(\frac{h}{2d}\right) \tag{9}$$

Following substitutions is used to write the non-dimensionalised form of equation (8):

$$\theta = \frac{x}{R};\ \bar{h} = \frac{h}{C};\ \bar{z} = \frac{z}{\left(L/2\right)};\ \bar{p} = \frac{pC^2}{6\mu UR};\ \tau = \omega t;\ \bar{\mu} = \frac{\mu_{nf}}{\mu_{bf}}$$

The final non-dimensional equation obtained is expressed as:

$$\frac{\partial}{\partial\theta}\left[\bar{f}\left(\bar{h},\bar{d}\right)\frac{\partial\bar{p}}{\partial\theta}\right] + \left(\frac{D}{L}\right)^2\frac{\partial}{\partial\bar{z}}\left[\bar{f}\left(\bar{h},\bar{d}\right)\frac{\partial\bar{p}}{\partial\bar{z}}\right] = \bar{\mu}\frac{\partial\bar{h}}{\partial\theta} + 2\bar{\mu}\frac{\partial\bar{h}}{\partial\tau} \tag{10}$$

where,

$$\bar{f}\left(\bar{h},\bar{d}\right) = \bar{h}^3 - 12\bar{d}^2\bar{h} + 24\bar{d}^3\tanh\left(\frac{\bar{h}}{2\bar{d}}\right) \tag{11}$$

For a dynamic state condition, the Reynolds equation in its non-dimensional form is expressed in Equation (10). The attitude angle ψ_0 and eccentricity ratio ε_0 are considered for the steady-state condition. If the journal undergoes whirling about its mean position with a small amplitude, and the system is perturbed to the first order while neglecting higher-order terms, the lubricant film thickness and pressure can be expressed in non-dimensional form as follows [14]:

$$\bar{h} = \bar{h}_0 + \varepsilon_1 e^{i\omega\tau}\cos\theta + \varepsilon_0\psi_1 e^{i\omega\tau}\sin\theta \tag{12}$$

$$\bar{p} = \bar{p}_0 + \varepsilon_1 e^{i\omega\tau}\bar{p}_1 + \varepsilon_0\psi_1 e^{i\omega\tau}\bar{p}_2 \tag{13}$$

By substituting $\bar{h}$ and $\bar{p}$ into Equation (10) and equating the coefficients of ε_0, $\varepsilon_1 e^{i\omega\tau}$ and $\varepsilon_0\psi_1 e^{i\omega\tau}$, a set of equations is obtained by neglecting higher-order terms. These equations are represented as Equations (14), (15), and (16).

The static pressure distribution is described by Equation (14), while the dynamic pressure components are described by Equations (15) and (16) for each lobe separately:

$$\frac{\partial}{\partial\theta}\left(f\left(\bar{h},\bar{d}\right)\frac{\partial\bar{p}_0}{\partial\theta}\right)+\left(\frac{D}{L}\right)^2\frac{\partial}{\partial\bar{z}}\left(f\left(\bar{h},\bar{d}\right)\frac{\partial\bar{p}_0}{\partial\bar{z}}\right)=\bar{\mu}\frac{\partial\bar{h}_0}{\partial\theta} \tag{14}$$

$$\frac{\partial}{\partial\theta}\left(\bar{f}\left(\bar{h},\bar{d}\right)\frac{\partial\bar{p}_1}{\partial\theta}\right)+\left(\frac{D}{L}\right)^2\frac{\partial}{\partial\bar{z}}\left(\bar{f}\left(\bar{h},\bar{d}\right)\frac{\partial\bar{p}_1}{\partial\bar{z}}\right)+3\frac{\partial}{\partial\theta}\left(\bar{h}_0^{\,2}\frac{\partial\bar{p}_0}{\partial\theta}\cos\theta\right)+3\left(\frac{D}{L}\right)^2\frac{\partial}{\partial\bar{z}}\left(\bar{h}_0^{\,2}\frac{\partial\bar{p}_0}{\partial\bar{z}}\cos\theta\right) \tag{15}$$
$$=-\bar{\mu}\sin\theta+2\bar{\mu}i\omega\cos\theta$$

$$\frac{\partial}{\partial\theta}\left(\bar{f}\left(\bar{h},\bar{d}\right)\frac{\partial\bar{p}_2}{\partial\theta}\right)+\left(\frac{D}{L}\right)^2\frac{\partial}{\partial\bar{z}}\left(\bar{f}\left(\bar{h},\bar{d}\right)\frac{\partial\bar{p}_2}{\partial\bar{z}}\right)+3\frac{\partial}{\partial\theta}\left(\bar{h}_0^{\,2}\frac{\partial\bar{p}_0}{\partial\theta}\sin\theta\right)+3\left(\frac{D}{L}\right)^2\frac{\partial}{\partial\bar{z}}\left(\bar{h}_0^{\,2}\frac{\partial\bar{p}_0}{\partial\bar{z}}\sin\theta\right) \tag{16}$$
$$=\bar{\mu}\cos\theta+2\bar{\mu}i\omega\sin\theta$$

The equation (14), (15) and (16) are solved by FDM using central difference method to obtain static and dynamic pressures. Which are expressed in equation (17), (18) and (19).

$$\bar{p}_{0_{i,j}}=\frac{\left[C_1\left(\bar{p}_{0_{i+1,j}}+\bar{p}_{0_{i-1,j}}\right)+C_0C_1\left(\bar{p}_{0_{i,j+1}}+\bar{p}_{0_{i,j-1}}\right)+C_2\left(\bar{p}_{0_{i+1,j}}-\bar{p}_{0_{i-1,j}}\right)+C_3\right]}{2C_1\left[1+C_0\right]} \tag{17}$$

$$\bar{p}_{1_{i,j}}=\frac{\left[\begin{array}{l}C_1\left(\bar{p}_{1_{i+1,j}}+\bar{p}_{1_{i-1,j}}\right)+C_0C_1\left(\bar{p}_{1_{i,j+1}}+\bar{p}_{1_{i,j-1}}\right)+C_2\left(\bar{p}_{1_{i+1,j}}-\bar{p}_{1_{i-1,j}}\right)-C_4\left(\bar{p}_{0_{i+1,j}}-\bar{p}_{0_{i-1,j}}\right)+\\ C_5\left(\bar{p}_{0_{i+1,j}}-2\bar{p}_{0_{i,j}}+2\bar{p}_{0_{i-1,j}}\right)+C_0C_5\left(\bar{p}_{0_{i,j+1}}-2\bar{p}_{0_{i,j}}+2\bar{p}_{0_{i,j-1}}\right)+C_6\end{array}\right]}{2C_1\left[1+C_0\right]} \tag{18}$$

$$\bar{p}_{2_{i,j}}=\frac{\left[\begin{array}{l}C_1\left(\bar{p}_{2_{i+1,j}}+\bar{p}_{2_{i-1,j}}\right)+C_0C_1\left(\bar{p}_{2_{i,j+1}}+\bar{p}_{2_{i,j-1}}\right)+C_2\left(\bar{p}_{2_{i+1,j}}-\bar{p}_{2_{i-1,j}}\right)+C_7\left(\bar{p}_{0_{i+1,j}}-\bar{p}_{0_{i-1,j}}\right)+\\ C_8\left(\bar{p}_{0_{i+1,j}}-2\bar{p}_{0_{i,j}}+2\bar{p}_{0_{i-1,j}}\right)+C_0C_8\left(\bar{p}_{0_{i,j+1}}-2\bar{p}_{0_{i,j}}+2\bar{p}_{0_{i,j-1}}\right)-C_9\end{array}\right]}{2C_1\left[1+C_0\right]} \tag{19}$$

where,

$$C_0=\left(\frac{D}{L}\right)^2\left(\frac{\Delta\theta}{\Delta\bar{z}}\right)^2;\ C_1=\bar{f}\left(\bar{h},\bar{d}\right);\ C_2=\frac{1}{2}\bar{f}'\left(\bar{h},\bar{d}\right)(\Delta\theta);C_3=\bar{\mu}\varepsilon\sin\theta(\Delta\theta)^2;$$

$$C_4=\frac{3}{2}\Delta\theta\bar{h}_0\sin\theta\left(\bar{h}_0+2\varepsilon\cos\theta\right);C_5=3\bar{h}_0^{\,2}\cos\theta;C_6=\left(\sin\theta-2i\omega\cos\theta\right)\bar{\mu}(\Delta\theta)^2;$$

$$C_7=\frac{3}{2}\Delta\theta\bar{h}_0\left(\bar{h}_0\cos\theta-2\varepsilon\sin^2\theta\right);C_8=3\bar{h}_0^{\,2}\sin\theta;\ C_9=\left(\cos\theta+2i\omega\sin\theta\right)\bar{\mu}(\Delta\theta)^2$$

For static and dynamic pressure following boundary condition used.

$$\frac{\partial\bar{p}_i}{\partial\theta}=0 \text{ and } \bar{p}_i=0 \text{ at } \theta=\theta_r;$$

$$\bar{p}_i\left(\theta,\bar{z}\right)=0 \text{ when } \theta_s\le\theta\le\theta_e \qquad (20)$$

where, $\bar{p}_i=\bar{p}_0,\bar{p}_1,\bar{p}_2$ and

The pressure distribution equations, expressed in non-dimensional form, are solved using the finite difference method with a central difference approach. The entire bearing is divided into two halves, and each half is further discretized into a grid of 88 × 16. Here, 88 grids represent the circumferential direction, while 16 grids represent the axial direction. Due to the symmetry of the pressure distribution about the bearing's central line, only one-half of the bearing is considered for analysis. For numerical integration, the Gauss-Seidel method is employed in combination with the successive over-relaxation technique to ensure boundary conditions are satisfied.

$$(p_{i,j})_{new}=(p_{i,j})_{old}+(Error)_{i,j}\times orf \qquad (21)$$

Equation (22) represents convergence criterion:

$$\frac{\left|\left(\sum\bar{p}_{i,j}\right)_{N-1}-\left(\sum\bar{p}_{i,j}\right)_N\right|}{\left|\left(\sum\bar{p}_{i,j}\right)_N\right|}\le10^{-6} \qquad (22)$$

Equation (23) gives dynamic load component along vertical and horizontal directions due to dynamic pressure component $\bar{p}_1$ and $\bar{p}_2$.

$$\bar{W}_{z1}=\int_{\theta_s}^{\theta_e}\int_0^1\bar{p}_1\sin\theta d\theta d\bar{z};\ \bar{W}_{z2}=\int_{\theta_s}^{\theta_e}\int_0^1\bar{p}_2\sin\theta d\theta d\bar{z};\bar{W}_{x1}=\int_{\theta_s}^{\theta_e}\int_0^1\bar{p}_1\cos\theta d\theta d\bar{z};\ \bar{W}_{x2}=\int_{\theta_s}^{\theta_e}\int_0^1\bar{p}_2\cos\theta d\theta d\bar{z}; \qquad (23)$$

To ensure the horizontal component is zero, the attitude angle must be adjusted for each eccentricity ratio. This indicates that the load is applied solely in the vertical direction. The stiffness and damping coefficients (both direct and cross-coupled) in their non-dimensional form are derived by separating the real and imaginary components of the vertical and horizontal loads. Equation (24) represents both the direct and cross-coupled stiffness and damping coefficients.

$$\bar{K}_{xx}=-\mathrm{Re}(\bar{W}_{x1});\ \bar{K}_{xz}=-\mathrm{Re}(\bar{W}_{x2});\bar{K}_{zx}=-\mathrm{Re}(\bar{W}_{z1});\ \bar{K}_{zz}=-\mathrm{Re}(\bar{W}_{z2})$$
$$\bar{C}_{xx}=-\mathrm{Im}(\bar{W}_{x1});\ \bar{C}_{xz}=-\mathrm{Im}(\bar{W}_{x2});\bar{C}_{zx}=-\mathrm{Im}(\bar{W}_{z1});\ \bar{C}_{zz}=-\mathrm{Im}(\bar{W}_{z2}) \qquad (24)$$

Non-dimensional friction variable,Sommerfeld number and flow coefficient are given as:

$$\bar{f} = f\left(\frac{R}{C}\right) = \frac{\int_0^{2\pi}\left(3\bar{h}\frac{\partial \bar{p}_0}{\partial \bar{z}} + \frac{\bar{\mu}}{\bar{h}_0}\right)d\theta}{6\bar{W}} \tag{25}$$

$$S = \frac{1}{6\pi\bar{W}} \tag{26}$$

$$\bar{q}_z = \frac{1}{2}\left(\frac{D}{L}\right)^2 \int_0^{2\pi} \frac{\bar{f}\left(\bar{h},\bar{d}\right)}{\bar{\mu}}\frac{\partial \bar{p}_0}{\partial \bar{z}}\,d\theta \tag{27}$$

3. RESULTS AND DISCUSSION:

3.1 Validation:

Due to the lack of standard results for a three-lobe bearing operating with a non-Newtonian lubricant under the couple stress model, the present results for the basic model are validated against those of Lund and Thomsen [2], who studied a three-lobe bearing with a Newtonian lubricant.

Table 1:*Comparison of Non-Dimensional Steady State and Dynamic Performance Parameters of Three-Lobe Fluid film Bearings for Newtonian Lubricant.*

Characteristics	$\varepsilon = 0.103$		$\varepsilon = 0.285$		$\varepsilon = 0.441$	
	Present	Lund and Thomsen [2]	Present	Lund and Thomsen [2]	Present	Lund and Thomsen [2]
ϕ	65.08	60.95	59.46	58.22	48.38	47.19
S	0.547	0.574	0.137	0.138	0.035	0.034
Q	0.142	0.139	0.177	0.173	0.232	0.232
K_{xx}	7.08	7.24	5.36	5.54	9.23	9.70
K_{xz}	8.08	8.55	4.11	4.22	4.56	4.65
K_{zx}	-7.56	-7.90	-2.16	-2.12	0.05	0.11
K_{zz}	4.26	4.24	2.03	1.92	1.48	1.42
C_{xx}	19.94	20.73	10.22	10.39	9.86	10.03
$C_{xz} = C_{zx}$	-0.51	-0.37	0.96	0.98	1.70	1.67
C_{zz}	13.41	14.27	3.84	3.81	1.32	1.23

The current results are in strong agreement with established published data for various models. After successful validation, the basic code was expanded to include a three-lobe journal bearing

with a couple stress model using nanolubricant. The results and discussion are presented in the following section.

3.2 Three-lobe fluid film bearing:

3.2.1 Steady-state performance parameter

Figure 2 displays the 3-dimensional pressure profile for the fixed parameters. Figure 3 presents the static pressure in non-dimensional form at the bearing's mid-plane along the circumferential node. The couple stress parameter is set to$d$=0.4and$\frac{L}{D}=1$, and the percentage of solid nanoparticles is varied from 0% to 2%. From the figure, it is evident that as the nanoparticle concentration in the nanolubricant increases, the pressure also increases. The most significant rise in pressure is observed when the nanoparticle volume fraction exceeds 0.5% (volume fraction of 0.005).

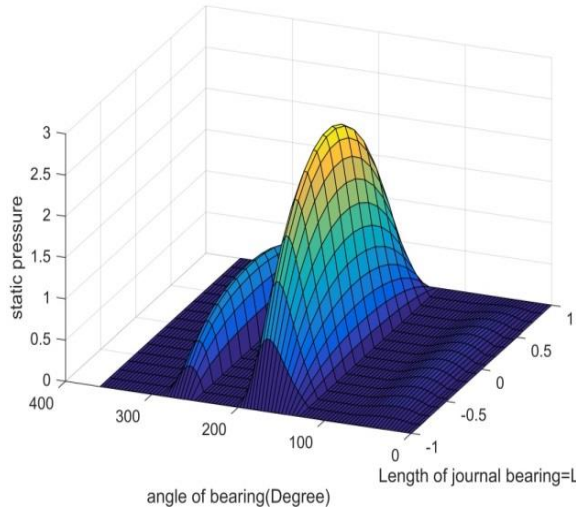

Figure 2:*Pressure profile of three-lobe bearing operating with non-Newtonian lubricant with d=0.4, eccentricity ratio=0.203 and volume fraction of nanoparticle=0.001*

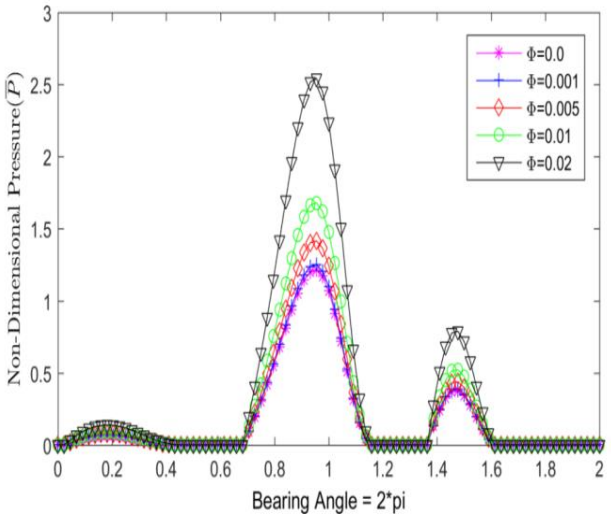

Figure 3: *Hydrodynamic pressure distributions at bearing mid-plane for different nano-particle volume fractions at an eccentricity ratio of 0.203 and couple stress parameter of 0.2.*

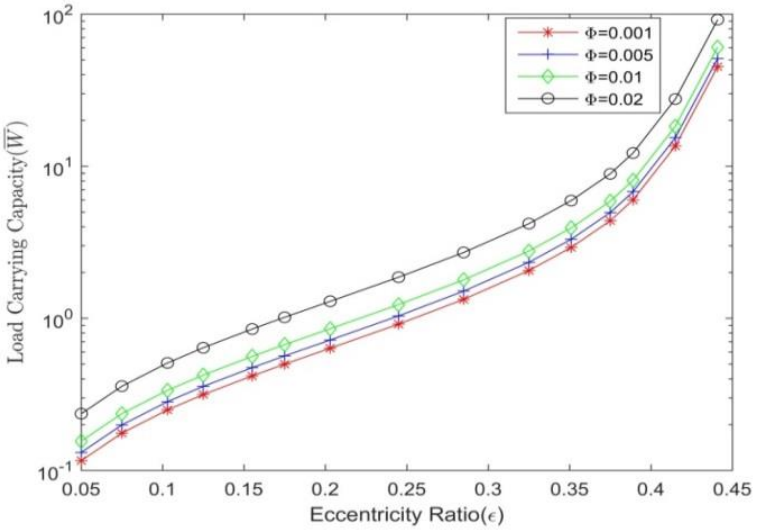

Figure 4: *Variation in load carrying capacity with volume fraction of nanoparticle.*

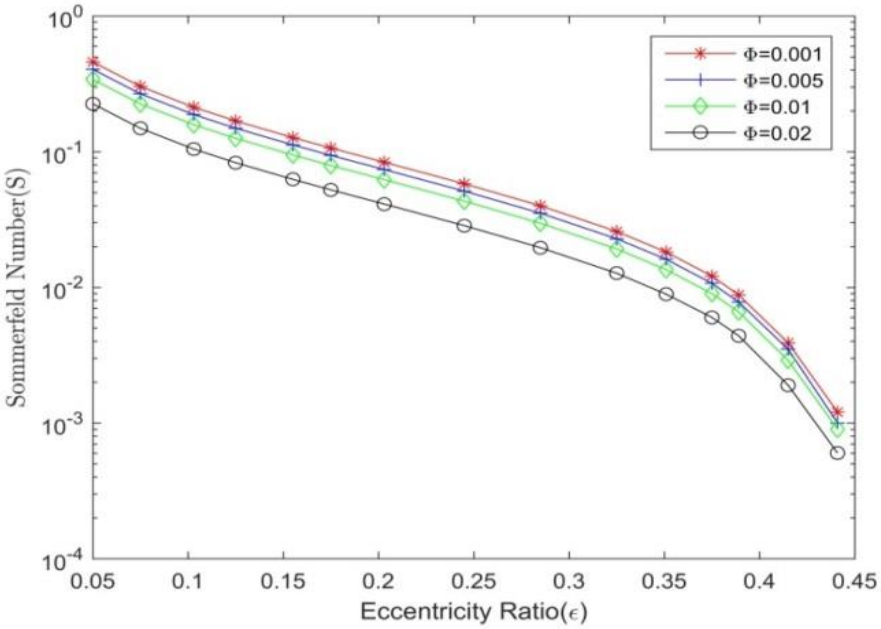

Figure 5: *Variation in Sommerfeld number with volume fraction of nanoparticle.*

As the percentage of solid structured nanoparticles in the base lubricant increases, it impacts the steady-state parameters of the fluid film bearing. These effects are illustrated in Figures 4 through 7. With the rise in solid nanoparticle concentration in the base fluid, there is an enhancement in hydrodynamic pressure, leading to an increase in the load-carrying capacity, as shown in Figure 4. The load-carrying capacity and Sommerfeld number are mathematically related and inversely proportional. Therefore, as the concentration of solid nanoparticles increases, the Sommerfeld number decreases, as depicted in Figure 5.

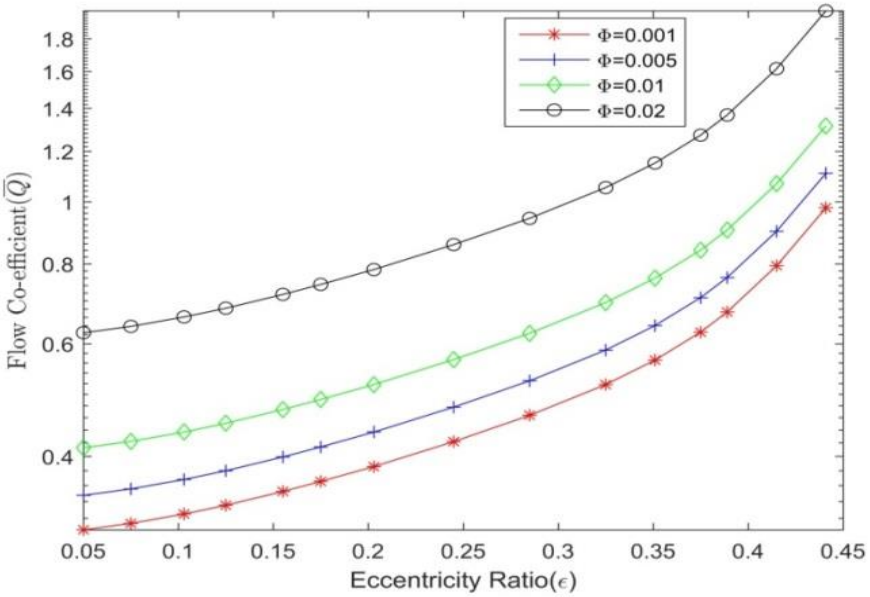

Figure 6:*Variation in floe coefficient with volume fraction of nanoparticle.*

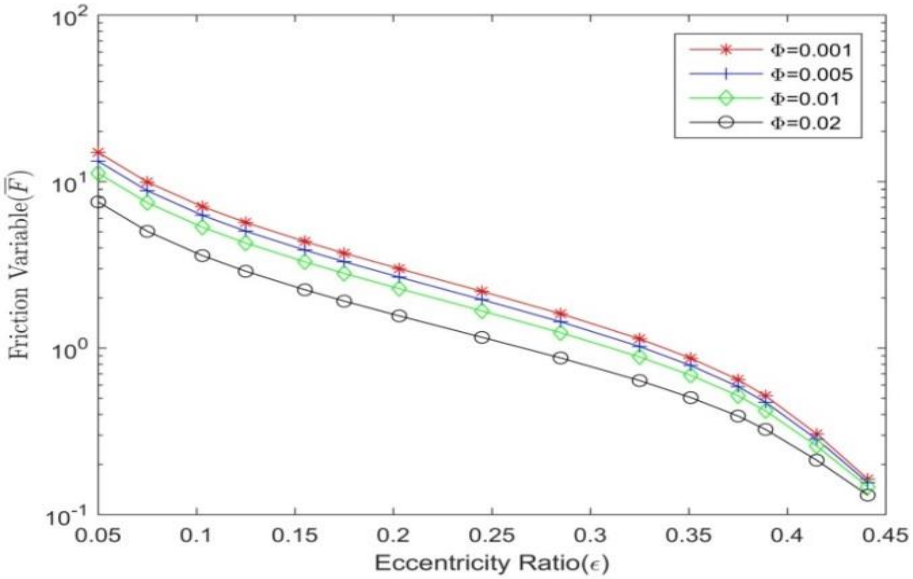

Figure 7: *Variation in friction variable with volume fraction of nanoparticle.*

Figure 6 shows the variation in flow coefficient with concentration of solid nanoparticle in base fluid. With increase in concentration of nanoparticle, flow coefficient increases. At the same time it also increases with increase in eccentricity ratio for a fixed percentage of solid nanoparticles in base fluid. Under normal circumstances in journal bearing, heavy friction occurs during startup and slows down of shaft. During these situations solid nanoparticle starts behaving as a rolling

element between shaft and bearing which drastically reduces the friction. Hence with increase in concentration of solid particles in base lubricant the friction variable decreases as depicted in Figure 7.

3.2.2 Dynamic Coefficients

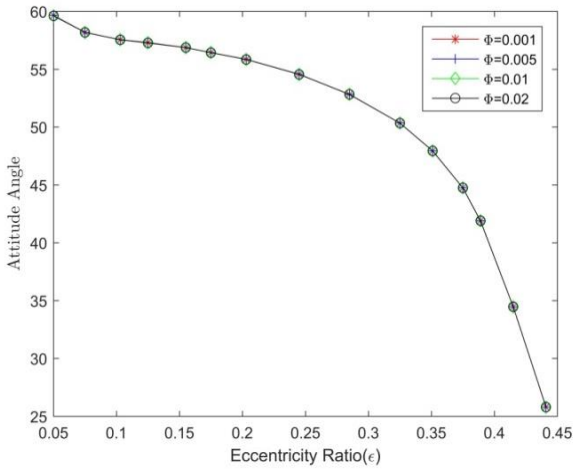

Figure 8: *Variation in attitude angle with volume fraction of nanoparticle.*

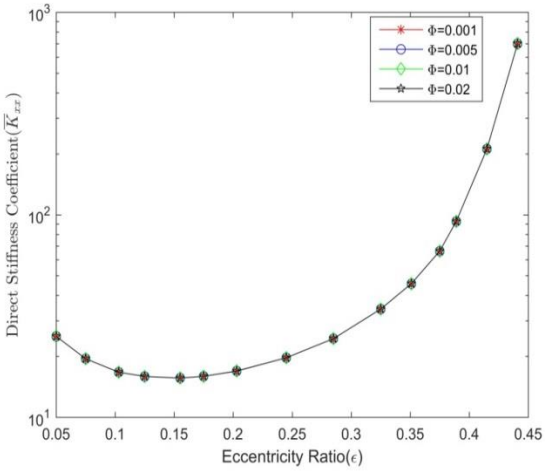

Figure 9: *Variation in direct stiffness coefficient with volume fraction of nanoparticle.*

As the concentration of nanoparticles changes, the load varies in both the horizontal and vertical directions. The ratio between the horizontal and vertical components influences the attitude angle. In this case, the load changes in such a way that the attitude angle remains constant, as shown in Figure 8.

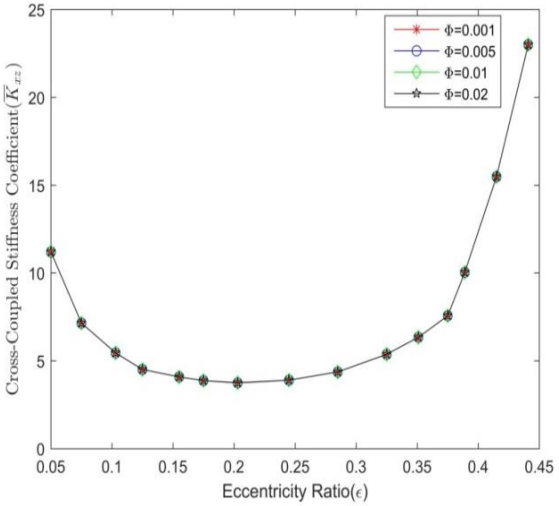

Figure 10: *Variation in cross coupled stiffness coefficient with volume fraction of nanoparticle.*

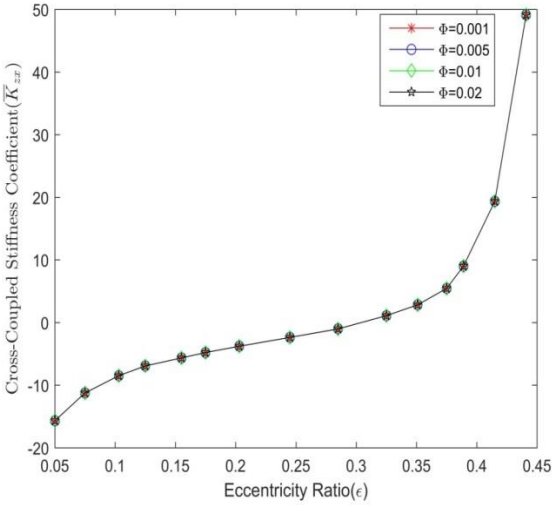

Figure 11: *Variation in cross coupled stiffness coefficient with volume fraction of nanoparticle.*

Figures 10 and 11 illustrate the variation in the cross-coupled stiffness coefficient as a function of the nanoparticle volume fraction. The influence of solid nanoparticle concentration in the base fluid on both stiffness and damping coefficients both direct and cross-coupled can be seen in Figures 9 through 16. The behavior of the dynamic coefficients differs significantly from that of the steady-state parameters. As the eccentricity ratio increases, the dynamic coefficient also increases for a given concentration. However, the dynamic coefficients do not show any variation with changes in the concentration of solid nanoparticles in the base fluid.

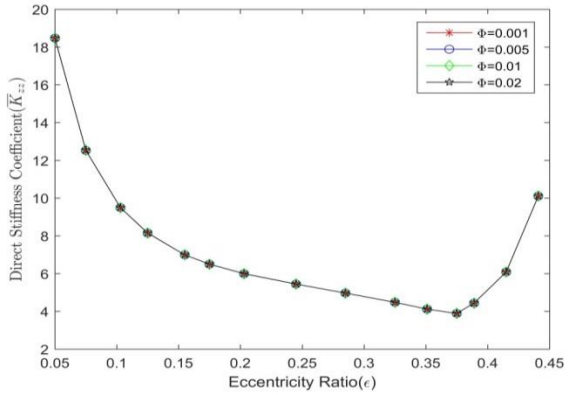

Figure 12: *Variation in direct stiffness coefficient with volume fraction of nanoparticle.*

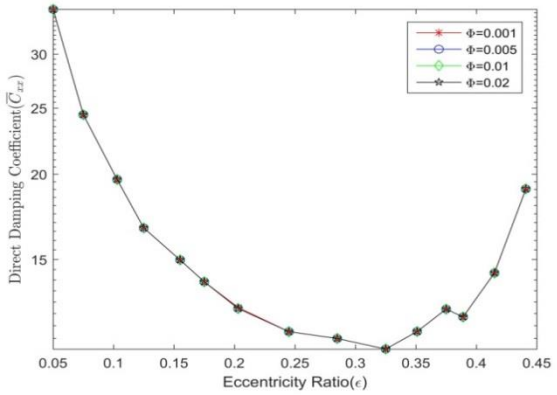

Figure 13: *Variation in direct damping coefficient with volume fraction of nanoparticle.*

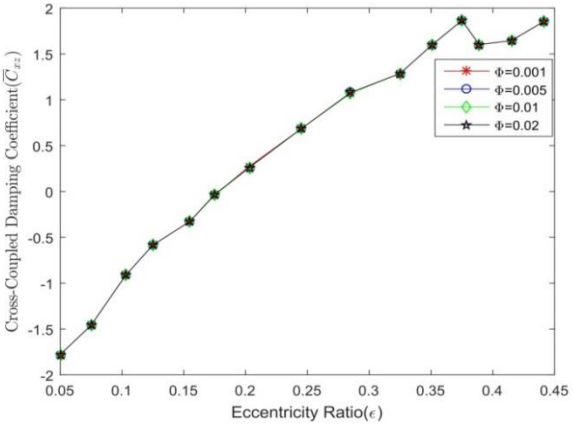

Figure 14: *Variation in cross coupled damping coefficient with volume fraction of nanoparticle.*

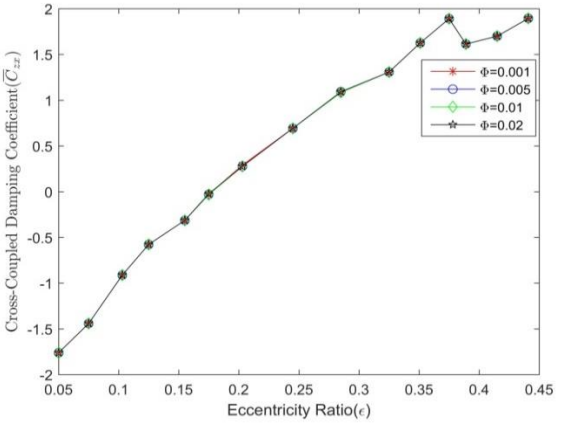

Figure 15: *Variation in cross coupled damping coefficient with volume fraction of nanoparticle.*

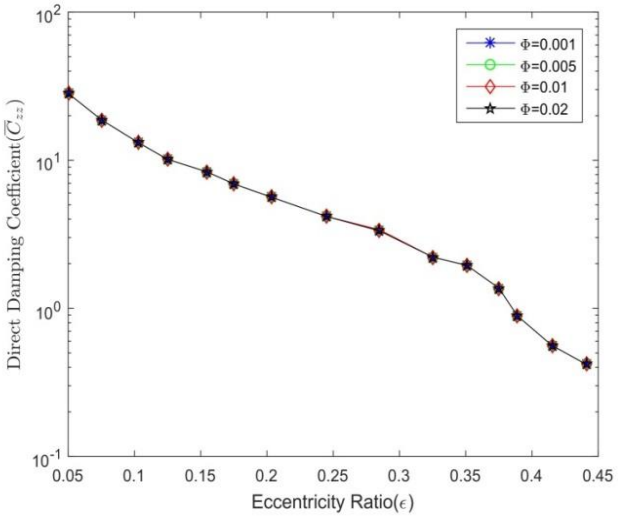

Figure 16:*Variation in direct damping coefficient with volume fraction of nanoparticle.*

The coefficients C_6 and C_9 are functions of the concentration of solid particles in the base lubricant, but they do not depend on other factors such as P_1 and P_2. The only parameter influencing the stiffness and damping coefficients is dynamic pressure. This may explain why the dynamic coefficients do not change with the concentration of solid particles in the base fluid.

4. CONCLUSIONS:

The impact of solid nanoparticle concentration in the base fluid on bearing performance parameters is significant. An increase in the concentration of solid nanoparticles in the lubricant enhances load capacity and leads to a reduction in friction. Additionally, the flow coefficient shows an increase with both higher eccentricity ratios and greater nanoparticle concentration in the base fluid. Throughout these changes, the couple stress remains constant. The results also indicate that as the solid nanoparticle concentration increases, the non-dimensional pressure rises, with a more noticeable increase when the volume fraction exceeds 0.005, as shown in Figure 3. The stiffness and damping coefficients of the bearing remain unchanged with varying nanoparticle concentration. Therefore, by adjusting nanoparticle concentration, the static characteristics of a three-lobe journal bearing can be improved without affecting its dynamic performance or stability.

While traditional lubricants are typically Newtonian, non-Newtonian lubricants are more commonly used, prompting research into nano-fluids as alternative lubricants. The findings of this study are expected to be valuable for future advancements in this area of research.

REFERENCES:

[1] S. C. Soni, R. Sinhasan, and D. V. Singh, "Performance characteristics of noncircular bearings in laminar and turbulent flow regimes," *ASLE Transactions*, vol. 24, no. 1, pp. 29–41, 1981.

[2] J. W. Lund and K. K. Thomson, "A calculation method and data for the dynamic coefficient of oil-lubricated journal bearings," *Proceedings of the ASME Design and Engineering. Conference*, pp. 1–28, New York, NY, USA, 1978.

[3] A. Singh and B. K. Gupta, "Static and dynamic properties of oil films in displaced centres elliptical bearings," *Proceedingsof the Institution of Mechanical Engineers, Part C: Journal ofMechanical Engineering Science*, vol. 197, no. 3, pp. 159–165, 1983.

[4] A. Kumar, R. Sinhasan, and D. V. Singh, "Performance characteristics of two-lobe hydrodynamic journal bearings," *Journal of Tribology*, vol. 102, no. 4, pp. 425–429, 1980.

[5] T. T. Ariman, N. D. Sylvester, "Microcontinuum fluid mechanics-A review", *International Journal of Engineering Science,* 1973; 11:905-30.

[6] T. T. Ariman, N. D. Sylvester, "Application of microcontinuum fluid mechanics", *International Journal of Engineering Science,* 1974; 224:194-201.

[7] V. K. Stokes, "Couple stresses in fluids", *Physics of fluids* 1966; 9:1709-15.

[8] J. R. Lin, "Squeeze film characteristics of finite journal bearing: couple stress fluid model", *Tribology International,* 1998; 31:201-7.

[9] XI Wang, K. Q. Zhu, S. Z. Wen, "on the performance of dynamically loaded journal bearings lubricated with couple stress fluids", *Tribology International,* 2002; 35:185-91.

[10] XI Wang, KQ Zhu, S. Z. Wen, "Thermohydrodynamic analysis of journal bearings lubricated with couple stress fluids", *Tribology International,* 2001; 34:335-43.

[11] U. M. Mokhiamer, W. A. Crosby, H. A. El-Gamal, "A study of journal bearing lubricated by fluids with couple stress considering the elasticity of liner", *Wear* 1999; 224:194-201.

[12] J. R. Lin, "Effect of couple stresses on the lubrication of finite journal bearing", *Wear* 1997; 206:171-8.

[13] A. Kumar and S. K. Kakoty, "Effect of Dam Depth and Relief Track Depth on Steady-State and Dynamic Performance Parameters of 3-Lobe Pressure Dam Bearing," *Advances in Tribology*,

[14] S. Das, S. K. Guha and A. K Chattopadhyay, "Linear stability analysis of hydrodynamic journal bearings under micropolar lubrication", *Tribology International,* 2005; 38:500-507.